多次元の信号に拡張する処理を行う必要がある．まず計測信号 **x** から，始点を x_t として間引き間隔 τ で N 点抜き出す．同様の操作を，始点を τ ずつずらして m 回行い，m 本の時系列を得る．それらを行ベクトルとして結合することで，m×N の埋め込み行列 **V** を得る．

$$\mathbf{V}=\begin{pmatrix} x_t & x_{t+\tau} & \cdots & x_{t+N\tau} \\ x_{t+\tau} & x_{t+2\tau} & \cdots & x_{t+(N+1)\tau} \\ \vdots & \vdots & \ddots & \vdots \\ x_{t+(m-1)\tau} & x_{t+m\tau} & \cdots & x_{t+(m+N-1)\tau} \end{pmatrix}$$

(m：次元数, N：信号の長さ, τ ：間引き間隔)

また，行列 **V** の 1 行目に異なる通過帯域幅を持つ FIR バンドパスフィルタをかけたものを参照信号 **r** として用いる．これは **V** の 1 行目の時系列を時刻の基準として与えるためである．

以上のようにして得られた行列 **V** と参照信号 **r** を用いて参照信号付きブラインド信号分離(BSSR)を行う．

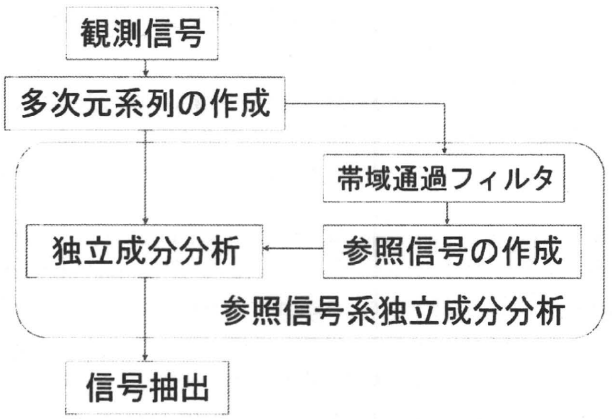

図 1　1 計測信号参照系独立成分分析の流れ

3. シミュレーション条件

原信号 s_1,s_2,s_3 として図 2 に示すような信号を用いた．このうち s_2 は実際に観測された胎児の心音時系列であり，サンプリングレートは 1000Hz である．これらの原信号を行列 $A=\begin{pmatrix}0.2 & 0.6 & 0.3\end{pmatrix}$ で混合したものを，観測時系列 **x** として用いた(図 3)．

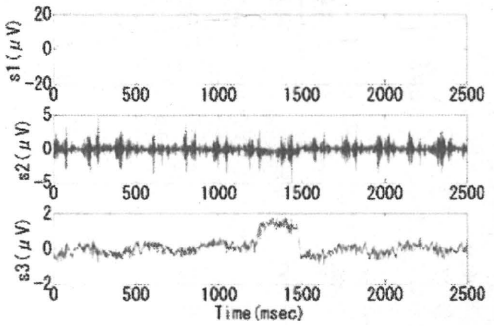

図 2　原信号 s_1,s_2,s_3

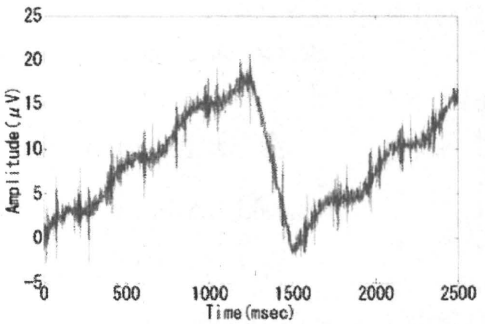

図 3　混合された信号時系列 **x**

この時系列 **x** から，長さ N=2300 の埋め込み行列 **V** を作成し，参照信号を 3 つ作成した(図 4)．作成に用いた FIR フィルタは通過帯域がそれぞれ以下の範囲になるように設計した．

r_1：0.1～1.0Hz，　r_2：5～498Hz，　r_3：1～5Hz

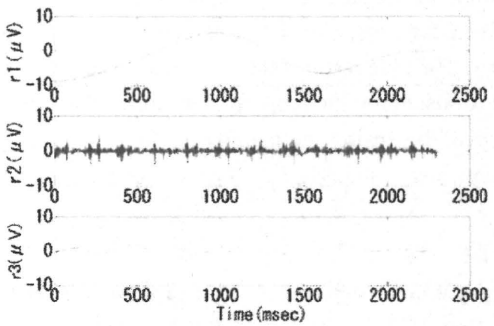

図 4　参照信号 **r**

4. シミュレーション結果

ここでは次元数 m および間引き間隔 τ を変化させて分離精度を調べる．

4.1. 次元数 m を変化させた場合

τ =1 の場合において m=5 から m=100 まで変化させて分離を行った．1～3ch で得られた信号と原信号との間で相関係数を調べ，それぞれの原信号との相関係数

が最も高い信号が現れたチャンネルを図 5 に，またそのときの相関係数を図 6 に示す．

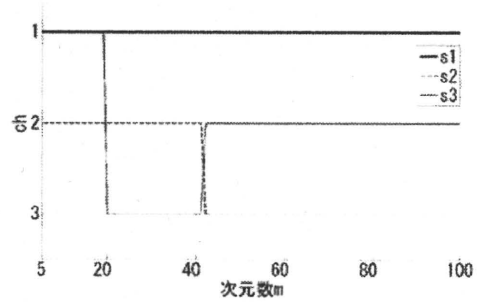

図 5　信号の出現チャンネル

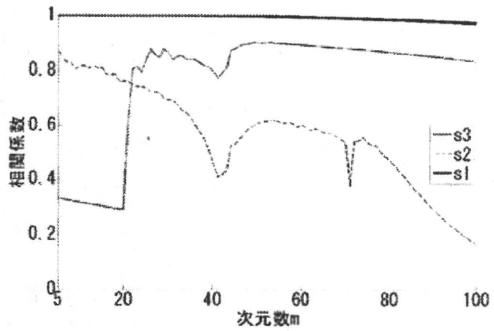

図 6　原信号と得られた信号との相関係数

図 5,6 より，3 つの信号が分離できたのは m≧20 のときである．また，m=41,42 の間で s_2, s_3 の出現チャンネルが入れ替わっており，そこで分離精度が落ち込んでいる．s_1 は m の値に関らず分離精度が高く，s_2 は m の増加とともに分離精度が落ちている．

以下に m=10(図 7),m=26(図 8),m=100(図 9)の場合の分離結果を示す．

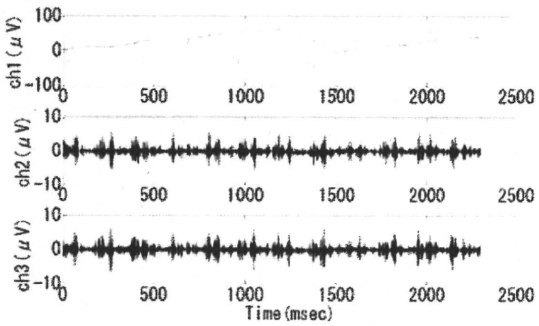

図 7　m=10 の場合の分離結果

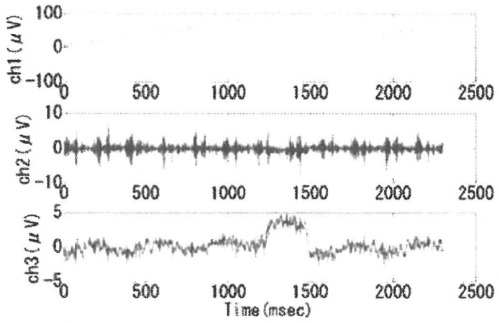

図 8　m=26 の場合の分離結果

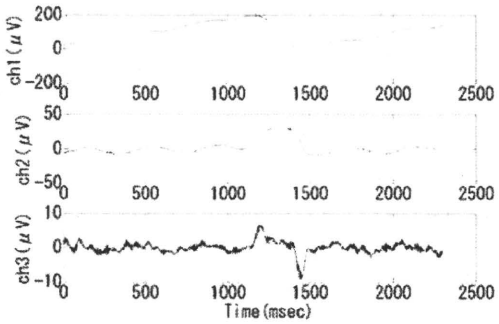

図 9　m=100 の場合の分離結果

図 7,8,9 を見ると，m=10 の場合は s_3 が分離できていない．m=100 の場合は ch3 にどの原信号とも波形の異なる信号が現れている．m=26 のときは比較的分離精度が高い．m≧20 の場合において，得られた信号と原信号との時間のずれを図 10 に示す．このとき，得られた信号の時間軸をある範囲内でずらしていき，原信号との相関係数が最も高くなったときのずれの値を「時間軸のずれ」としている．

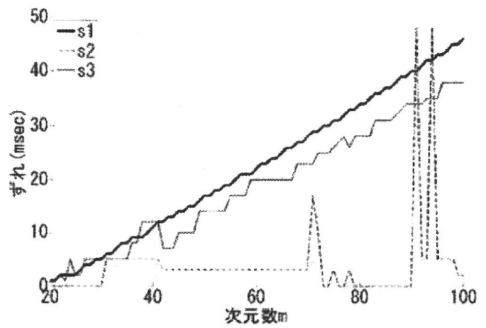

図 10　得られた信号と原信号との時間軸のずれ

s_1, s_3 のずれは次元数 m に比例しているように見える．s_2 は分離精度そのものが低いため，正確な時間軸のずれの値を求めるのが困難であり，次元数 m と時間ずれのシステマティックな関係性は見えなかった．

4.2. 間引き間隔τを変化させた場合

m=31 の場合においてτ=1 からτ=10 まで変化させて分離を行った．埋め込み行列 **V** は **x** を n=25000 まで延長した時系列から作成した．

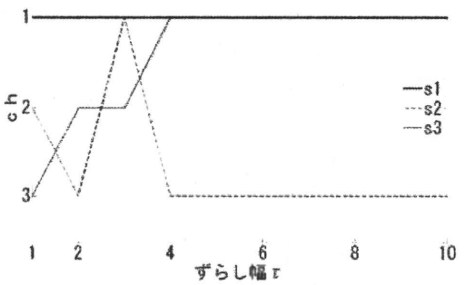

図 11　信号の出現チャンネル

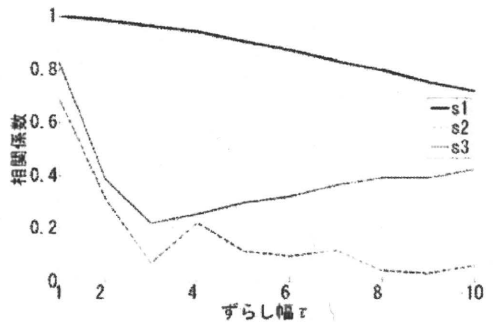

図 12　原信号と得られた信号との相関係数

3 つの信号が分離できたのはτ=1,2 の場合だけだった．相関係数はτ=1 の場合が最も高く，それ以外では s_1 以外の信号は分離できなかった．τ=2 の場合の分離信号を図 13 に示す．

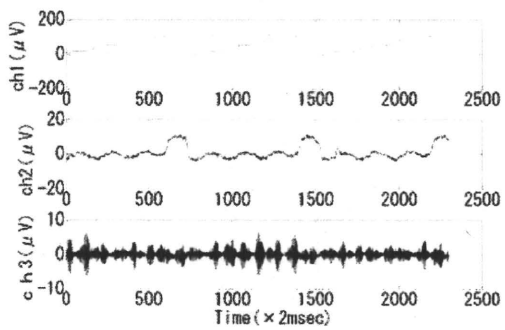

図 13　τ=2 の場合の分離結果

τ=2 ではτ=1 のときと比べて分離精度が下がったが，さらにτを大きくしていくと分離精度が上がるものと下がるものがあった．

5. 結論

次元数 m を変化させたときで，得られた信号と原信号との関係を調べると，相関係数と時間軸のずれがともに変化しているのが確認できた．図 6 をみると，次元数 m を増やすほど分離精度が向上するというわけではなく，s_1 のように m の値にあまり影響を受けずに高い精度で抽出できる信号もあれば，m の値がある範囲では分離精度が上がり，ある範囲では低下する信号もあった．また，図 10 より，時間のずれ方も各信号で異なっていることがわかる．

間引き間隔τについては，τ≧2 では s_1 以外の分離精度が低く，分離に有効なτの値もしくは範囲は見つけられなかったが，τを大きくすると分離精度が上がる信号が見られた．

これらの結果から，s_1 は時系列 **x** に含まれる成分のうちで，mやτを様々な値に設定しても，その値からできる埋め込み行列 **V** の各行の確率構造が変わりにくいものであり，そのような信号はこの手法で抽出しやすいといえる．このような性質を持った信号でなくても，mやτの値を適切に設定し，その埋め込み行列の各行で確率構造が変わらない信号ができれば，分離精度をより向上できるであろう．確率構造がある時間ずれに対して変わらない信号とは例えば，定常なノイズや，その時間ずれが自らの周期の整数倍である信号である．

今後はmとτを適切に設定してやることで，抽出したい信号に上記の定常性や周期性のような性質を持たせる手法について検討したい．

参考文献

[1] A.Jiménez-González, C.J.James, "Extracting sources from noisy abdominal phonograms :a single-channel blind source separation method," Medical and Biological Engineering, vol.47, no.6, pp.655-664, 2009.

[2] M.Sato, Y.Kimura, S.Chida, T.Ito, N.Katayama, K.Okamura, and M.Nakao, "A Novel Extraction Method of Fetal Electrocardiogram From the Composite Abdominal Signal", IEEE Trans. Biomed. Eng.,vol.54, no.1, pp.51-52, 2007.

30th Annual International IEEE EMBS Conference
Vancouver, British Columbia, Canada, August 20-24, 2008

Robustness of the Blind Source Separation with Reference against Uncertainties of the Reference Signals

Tomoyuki Netabayashi, Yoshitaka Kimura, Shinichi Chida, Takuro Ito, Kazunari Ohwada, Norihiro Katayama, Kunihiro Okamura, and Mitsuyuki Nakao, *Member, IEEE*

Abstract—**The fetal electrocardiogram (ECG) could provide clinical information concerning physiological conditions of the fetus. In order to extract fetal ECG, we proposed the novel algorithm, the blind source separation with reference (BSSR), which successfully extracts a complete waveform of QRS complex and avoids uncertainty in the order of the extracted signals. In the BSSR, the reference signal is supposed to be generated from the ultrasonic Doppler signal. Thus generated reference is expected to suffer from uncertainties in waveform and occurrence timing. Based on simulations, the BSSR is shown to have robustness against the uncertainties of reference signals. In addition, it is shown how the robustness depends on the order of power of correlation function between the reference and extracted signals, which composes a performance function of the BSSR.**

I. Introduction

A FETAL electrocardiogram (ECG) provides clinically significant information concerning physiological states of a fetus. For example, arrhythmias show the immaturity of fetal cardiac activity, and anoxia is known to alter the balance between the electrical polarization and repolarization of heart [1]. Ultrasonic measurements of physical motions of the heart could not provide the electrophysiological information. Nevertheless, the fetal ECG has not yet been popularly used in the clinical situations, because there is no low cost and reliable method to measure the fetal ECG. The magnetocardiogram (MCG) could directly monitor the electrical activity of fetal heart, which is measured by placing a SQUID probe close to the fetus over the mother's abdomen [2]. However, the MCG measurement needs a special large scale equipment [2]. Instead, the signal processing methods extracting the fetal ECG signal from the composite abdominal signal have been developed [3],[4]. Especially, the independent component analysis (ICA) or blind source separation (BSS) have been applied to this problem [5],[6]. In comparison with them, our proposed algorithm, BSSR (blind source separation with reference), realizes better performances in the following points [7]. The BSSR successfully extracts a complete waveform of QRS complex and avoids uncertainty in the order of the extracted signals. This algorithm is characterized by usage of the reference signal which mimics a source signal to be restored. For extracting ECG, the reference is a sequence of spike-like events each of which corresponds to a heart beat. Actually, the reference signal is supposed to be generated from the ultrasonic Doppler signal which is usually monitored in clinical diagnosis. According to our preliminary study, a generated reference signal from the Doppler signal is thought to suffer from uncertainties in waveform and occurrence timing, because the Doppler signals have inherently random nature in shape [8]. It is not clarified how these uncertainties affect performance of the BSSR.

In this paper, how performance of the BSSR depends on the uncertainties of the reference signals are clarified by simulations. In addition, it is investigated how this dependency is modified by the order of power of correlation function between the reference and extracted signals, which composes a performance function of the BSSR [7]. Through these simulation studies, permissible range of uncertainties of the reference is clarified for the BSSR. This result could provide necessary conditions for us to develop a generation method of the reference from the ultrasonic Doppler signal.

II. Algorithm of Blind Source Separation with Reference and Simulation Conditions

A. Algorithm of BSSR

The data are pre-whitened, i.e., the covariance matrix of the data is diagonalized [8]. The method is formulated as follows. Let us consider a situation that n source signals $\mathbf{s}=(s_1, s_2, \cdots, s_n)$ are observed as $\mathbf{x}=(x_1, x_2, \cdots, x_m)$ through a linear and immediate mixture $\mathbf{x}=A\mathbf{s}$, where A denotes the full rank mixing matrix of $m \times n$. Our purpose is to estimate A and $\mathbf{s}$. Here, the estimation of individual source signal is considered separately, $y=\mathbf{w}^T\mathbf{x}$, where y and $\mathbf{w}$ denote estimates of a source signal and the corresponding row vector of the estimated inverse of A, respectively. T denotes a transpose. Here, note that only a few sources are needed to be recovered out of m observations. They are fetal ECGs which consist of almost periodic sequence of pulse-like events. In this sense,

Manuscript received April 7, 2008. This work was supported in part by Special Coordination Funds for Promoting Science and Technology and by the "Academic Frontiers" Project for Private Universities (Kansei Fukushi Research Center of Tohoku Fukushi University) through a matching fund subsidy from the Ministry of Education, Culture, Sports, Science and Technology of Japan.

T.Netabayashi, N.Katayama, and M.Nakao are with Graduate School of Information Sciences, Tohoku University, Sendai 980-8579, Japan (corresponding author to provide phone & fax: +81-22-795-7157; e-mail: nakao@ ecei.tohoku.ac.jp).

Y.Kimura and T.Ito are with TUBERO, Tohoku University, Sendai 980-8575, Japan

S.Chida is with TESCO Co. Ltd., Sendai 980-0832, Japan

K.Ohwada is with Atom Medical Co. Ltd., Tokyo 113-0033, Japan

K.Okamura is with Graduate School of Medicine, Tohoku University, Sendai 980-8575, Japan

978-1-4244-1815-2/08/$25.00 ©2008 IEEE.

the situation is not a completely blind one. In order to aid the estimation, an artificial or observable signal closely related to the source signal to be recovered is referred to. Now, we think of estimating y which is highly correlated with the reference signal r under the constraint $|\mathbf{w}|=1$. This is realized by maximizing the Lagrangian:

$$L(\mathbf{w}) = \frac{1}{2k} E[y^{2k} r^{2k}] - \frac{\lambda}{2}(\mathbf{w}^T \mathbf{w} - 1), \qquad (1)$$

where $E[\ ]$ denotes an expectation, and λ is a Lagrange multiplier [7]. Here, the correlation $E[y^{2k} r^{2k}]$ is called "performance function" [9]. As a solution of (1), we have

$$\mathbf{w} = \frac{E[y^{2k-1} r^{2k} \mathbf{x}]}{E[y^{2k} r^{2k}]} . \qquad (2)$$

Actually, the following interations give the solutions.

$$\mathbf{w}_{n+1} = \frac{E[y_n^{2k-1} r^{2k} \mathbf{x}]}{E[y_n^{2k} r^{2k}]} \qquad (3)$$

$$y_{n+1} = \mathbf{w}_{n+1}^T \mathbf{x} .$$

The practical estimation is performed as follows. The initial value of $\mathbf{w}$ is given as a vector whose entries take ± 1 at random. This is only for starting algorithm with not so strong preference. The extraction is done in a segment-wise manner, where one segment is 5s (5,000 points). The expectation is realized by the temporal integration in the respective segment. k=2 unless otherwise stated. The details of our algorithm were explained in comparison with previously proposed methods elsewhere [7].

B. Simulation Conditions

For simulations, we use test source signals shown in Fig.1. Among them, ch.1-ch.3 are separated a priori from the actual composite abdominal signal. Note that 4th power of Gaussian noise resembles ECG in its statistical properties. The observed signal subject to separation is obtained through

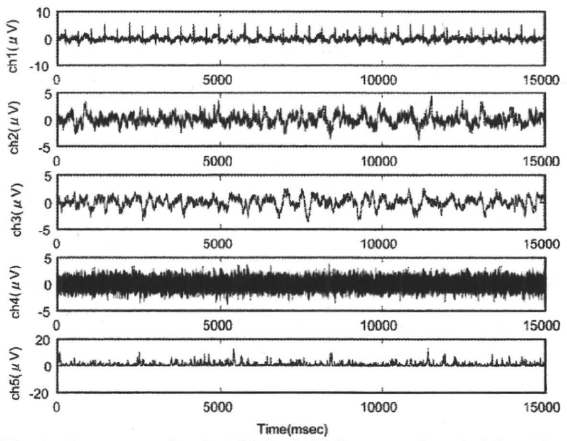

Fig. 1. Test source signals. ch1:fetal ECG separated a priori from the composite abdominal signal, ch2, ch3:residual signals separated a priori from the composite abdominal signal, ch4:Gaussian noise, ch5: 4th power of Gaussian noise.

operating an appropriate 5×5 mixing matrix ([0.203 0.0153 0.419 0.838 5.03; 0.199 0.747 0.846 0.0196 7.09; 0.604 0.445 0.525 0.681 4.29; 0.272 0.932 0.203 0.380 3.05; 0.199 0.466 0.672 0.832 1.90]) on the test source signal.

The reference signal is a sequence of spike-like event shaped by $\cos 2\pi(t-t_p)/d$, $|t-t_p| \le d/2$, where t denotes the time, t_p indicates the peak position of the reference event, and d denotes width of event. In order to include basic uncertainty, a timing of each event is randomly shifted following a uniform distribution around occurrence of R

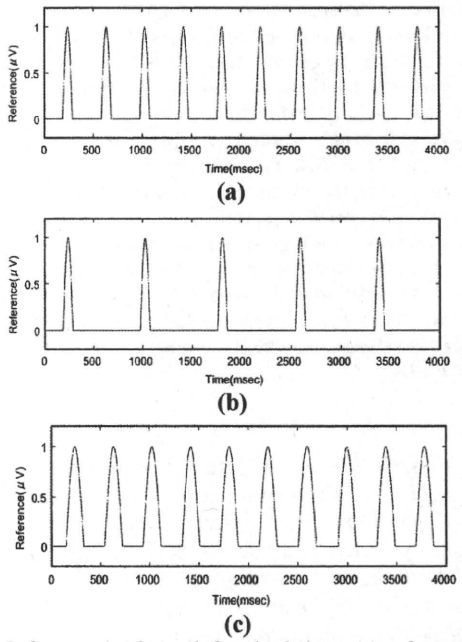

Fig.2. Reference signals used for simulations. **(a)** reference signal (d=100ms). **(b)** reference signal decimated by a rate of 0.5 (d=100ms). **(c)** reference signal consists of width-varied events (d=180ms)

wave of the fetal ECG in ch.1. Thus constructed reference signal is shown in Fig.2**(a)**. Furthermore, we add other types of uncertainty to this reference signal: decimation of reference events by a rate of 0.5 or 0.125 (Fig.2**(b)** for 0.5), and variation of event width 20ms or 180ms (Fig.2**(c)** for d=180ms).

III. Simulation Results

A. Fundamental Performance of BSSR

Fig.3**(a)** shows the fundamental performance of the BSSR against uncertainty in timing of reference event, where a correlation of the extracted signal with the ECG signal (source 1) is plotted as a function of the range of uniform distribution for random shifting. Simulations ran 50 times with different sample processes of noise signals (sources 4 and 5), and averaged results are shown. This plot indicates how the ECG signal is contained in each extracted channel. Naturally, it is desirable that a single channel exclusively contains the ECG signal. In this figure, the correlation in ch.1 is gradually degraded beyond the shift range of 40ms, and instead those in the other channels increase, i.e., the ECG signal becomes scattered over the channels. This result

indicates that full recovery of the ECG signal becomes difficult as the timing of reference event more largely deviates from the correct position. This could be understood from deterioration of the performance function as shown in Fig.3(**b**). That is, the performance function for the ECG signal monotonically decreases associated with an extension of shift range. In contrast, the 4th power of Gaussian noise (source 5) raises its performance function. This is due to highly randomized reference signal resembles the 4th power of Gaussian noise in a statistical sense. It is worth noting that the degradation of performance of ECG extraction coincides with an increase of the performance function for the source 5.

B. Performance of BSSR with decimated reference signals

Fig.4 shows how the 1/2 decimation of reference event affects the performance of the BSSR. In Fig.4(**a**), the correlation for ECG signal in ch.1 is shown to be retained until the shift range of 70ms, but to deteriorate little bit more rapidly than the case of no decimation. This could be understood from behavior of the performance function shown in Fig.4(**b**). Although the absolute value itself is almost halved, the performance function decreases with a similar rate to the case of no decimation. A distinct thing is that the build-up of performance function for the source 5 begins around the shift range of 70ms or larger, which coincides again with the collapse of correlation in ch.1. In the case of 1/8 decimation, value of the performance function for the ECG signal was an eighth of the case with a complete reference signal, and the build-up of the performance function for the source 5 began around the shift range of 120ms (the results were omitted). Although the correlation in ch.1 was always lower than 1, it decreased more gradually than the case with a complete reference as well as 1/2 decimation.

C. Performance of BSSR with varied width of reference event

Fig.5 shows the performance of the BSSR with the width of reference event d=180ms. Characteristically, the correlation in ch.1 is shown to be maintained close to 1 up to the shift range of 70ms, and to decrease rapidly beyond this critical range of shift. In addition, the correlations in ch.2 and ch.3 are built-up more rapidly in comparison with the

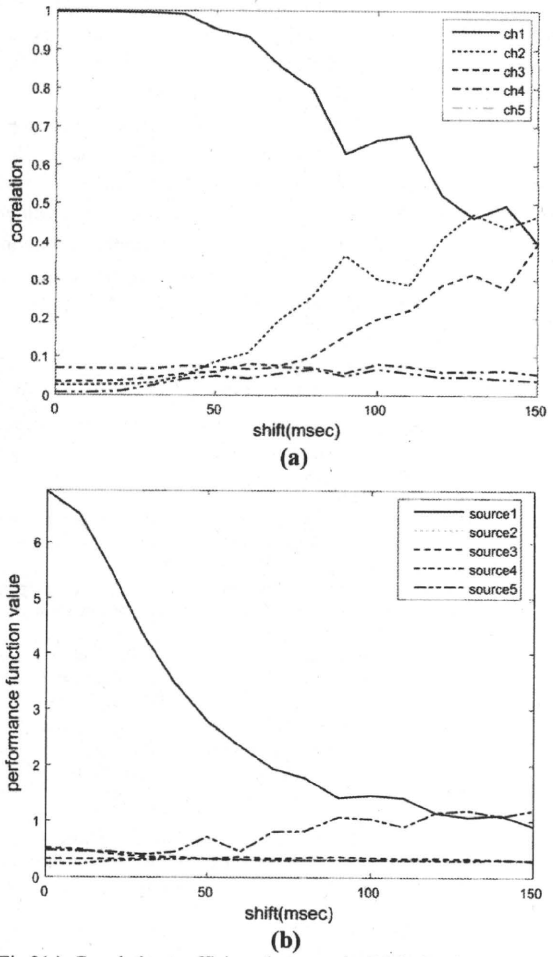

Fig.3(**a**) Correlation coefficients between the ECG signal and signals in the extracted channels. (**b**) Performance function for each extraction. Shift value indicates a deviation range from the center of the uniform distribution. d=100ms..

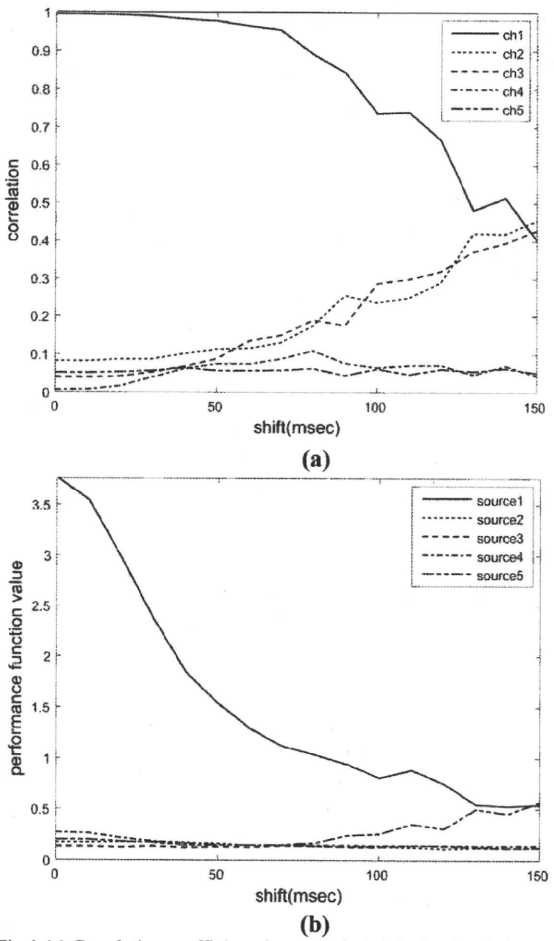

Fig.4 (**a**) Correlation coefficients between the ECG signal and signals in the extracted channels with 1/2 decimated reference signal. (**b**) Performance function for each extraction. Shift value indicates a deviation range from the center of the uniform distribution. d=100ms..

case of d=100ms. This wider range of shift allowing acceptable performance of the BSSR could be understood from the behavior of performance function. The performance function for the ECG signal more gradually decreases and that for the 4th power of Gaussian noise more rapidly increases in comparison with the case of d=100ms. In contrast, under the condition of d=20ms the correlations in ch.1 and in chs.2 and 3 were progressively reduced and built-up from a further smaller range of shift than d=100ms, respectively (the results were omitted here). As easily expected, the performance function for the ECG signal more steeply decreased under d=20ms than d=100ms.

D. Robustness of BSSR dependent on the order of performance function

In the previous simulations, the robustness of the BSSR against various kinds of uncertainties in the reference signal was investigated, which showed that the performance of the BSSR could be well understood based on the performance function. Naturally, the robustness of the BSSR is expected to depend on the order of the performance function which is denoted by $2k$. This dependency was examined by simulations. Here, the results are only summarized. As for k=1, although the performance function for the ECG signal dominated the others, the performance function for the Gaussian noise was relatively large, which could be responsible for the extraction performance that the ECG signal leaked into a few channels. As for k=4, the ECG signal significantly leaked into another channel in addition to ch.1 even under small range of shift over 30ms. This is possibly due to the fact that the performance function for the 4th power of Gaussian noise was rapidly built-up and exceeded that for the ECG signal over the shift of 30ms. In other words, it is difficult for the eighth power of correlation $E[y^8 r^8]$ to distinguish between the ECG signal and the 4th power of Gaussian noise.

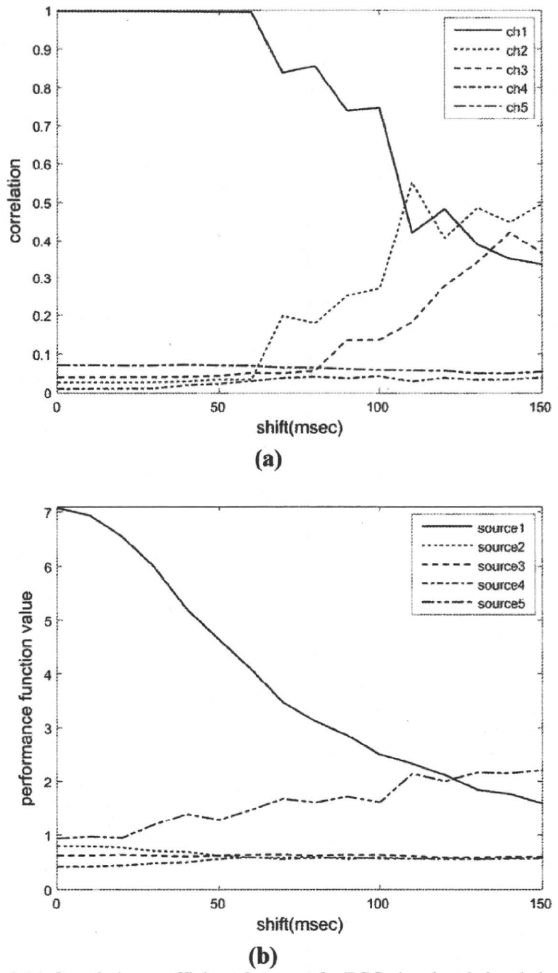

Fig.5 **(a)** Correlation coefficients between the ECG signal and signals in the extracted channels with the reference event width d=180ms. **(b)** Performance function for each extraction. Shift value indicates a deviation range from the center of the uniform distribution.

IV. Conclusion

Through the simulations, the BSSR was shown to have robustness against various kinds of uncertainties in the reference signal. The performance of the BSSR could be well understood in terms of the behavior of performance function. These results provide useful information concerning permissible uncertainties of the reference signal. In addition, because the performance of the BSSR depends on the order of the performance function, it could be a possible strategy that the order of the performance function is selected responsible for what kinds of noise are expected to be contained in observed signals. Generalization of our findings will be a future subject.

References

[1] E.M. Symonds, D. Sahota, and A. Chang, *Fetal Electrocardiology*. London: Imperial College Press, 2001.

[2] *Fetal Cardiogram Database*, Aug. 2004 [Online]. Available: http://bct.tn.utwente.nl

[3] A. Khamene and S. Negahdaripour, "A new method for the extraction of fetal ECG from the composite abdominal signal," *IEEE Trans. Biomed. Eng.*, vol.47, pp.507-516, April 2000.

[4] V. Zarzoso and A.K.Nandi, "Noninvasive fetal electrocardiogram extraction: Blind separation versus adaptive noise cancellation," *IEEE Trans. Biomed. Eng.*, vol.48, pp.12-18, Jan 2001.

[5] L. De Lathauwer, B. De Moor, and J. Vandewalle, "Fetal electrocardiogram extraction by blind source subspace separation," *IEEE Trans. Biomed. Eng.*, vol.47, pp.567-572, May 2000.

[6] M.J.O. Tayler, M.J. Smith, M. Thomas, A.R. Green, F. Cheng, S. Oseku-Afful, L.Y. Wee, N.M. Fisk, and H.M. Gardiner, "Non-invasive fetal electrocardiography in singleton and multiple pregnancies," *Int. J. Obstet. Gynaecol.*, vol.110, pp.668-678, July 2003.

[7] M.Sato, Y.Kimura, S.Chida, T.Ito, N.Katayama, K.Okamura, and M.Nakao, "A novel extraction method of fetal electrocardiogram from the composite abdominal signal," *IEEE Trans. Biomed. Eng.*, vol.54, pp.49-58, 2007.

[8] T. Netabayashi, "A method for extracting fetal ECG based on the BSSR," Master Thesis, GSIS, Tohoku Univ, 2008.

[9] A. Cichocki and S. Amari, *Adaptive Blind Signal and Image Processing*, West Sussex, U.K.: Wiley, 2002.

Development, Growth & Differentiation
The Japanese Society of Developmental Biologists

Develop. Growth Differ. (2011) **53**, 357–365 doi: 10.1111/j.1440-169X.2010.01235.x

Original Article

Differentiation of neuronal cells from NIH/3T3 fibroblasts under defined conditions

Zhuo Wang, Eriko Sugano, Hitomi Isago, Teru Hiroi, Makoto Tamai and Hiroshi Tomita*

Tohoku University Institute for International Advanced Interdisciplinary Research, 4-1 Seiryo-machi, Aoba-ku, Sendai 980-8575, Japan

We attempted to test whether the differentiated NIH/3T3 fibroblasts could be differentiated into neuronal cells without any epigenetic modification. First, a neurosphere assay was carried out, and we successfully generated neurosphere-like cells by floating cultures of NIH/3T3 fibroblasts in neural stem cell medium. These spheres have the ability to form sub-spheres after three passages, and express the neural progenitor markers Nestin, Sox2, Pax6, and Musashi-1. Second, after shifting to a differentiating medium and culturing for an additional 8 days, cells in these spheres expressed the neuronal markers β-tubulin and neurofilament 200 and the astrocytic marker glial fibrillary acidic protein (GFAP). Finally, after treating the spheres with all-trans retinoic acid and taurine, the expression of β-tubulin was increased and the staining of photoreceptor markers rhodopsin and recoverin was observed. The present study shows that NIH/3T3 fibroblasts can generate neurosphere-like, neuron-like, and even photoreceptor-like cells under defined conditions, suggesting that the differentiated non-neuronal cells NIH/3T3 fibroblasts, but not pluripotent cells such as embryonic stem cells or induced pluripotent stem cells, may have the potential to be transdifferentiated into neuronal cells without adding any epigenetic modifier. This transdifferentiation may be due to the possible neural progenitor potential of NIH/3T3 fibroblasts that remains dormant under normal conditions.

Key words: differentiation, neural progenitors, neuron, retinoic acid, taurine.

Introduction

Because of their ability to proliferate infinitely and differentiate into cells of all three germ layers, embryonic stem (ES) cells are regarded as superior potential donor cells for cell replacement to treat many diseases (Hoffman & Carpenter 2005; Takahashi & Yamanaka 2006), such as retinitis pigmentosa and age-related macular degeneration, which are typically characterized by the death of photoreceptors (Osakada *et al.* 2008). Photoreceptor replacement in the form of a cell-based therapeutic approach may aid in the restoration of vision.

Zhao *et al.* (2002) demonstrated that ES cell-derived neural progenitors expressed regulatory factors needed for retinal differentiation, and that a small subset of these cells differentiated along the photoreceptor lineage in response to retina-specific epigenetic cues. Ikeda *et al.* (2005) and Osakada *et al.* (2008) generated putative photoreceptors and RPE cells from rodent and primate ES cells by induction with defined factors.

However, in clinical application, the use of ES cells involves ethical problems and immune rejection. Jin *et al.* (2009) demonstrated partial mesenchymal stem cells obtained from umbilical cord blood were able to be differentiated into neuron-like cells or rhodopsin-positive cells *in vitro*. Recently, retinal cells have been generated from mouse- and human-induced pluripotent stem (iPS) cells by introducing four specific factors Oct3/4, Sox2, Klf4, and c-Myc (Takahashi & Yamanaka 2006; Hirami *et al.* 2009; Osakada *et al.* 2009).

Even though the generation and application of iPS cells made it possible to treat patients with their own cell-derived retinal cells, which may resolve the problem of immune rejection, some questions still remain. For example, the introduction of viral vectors and oncogenes c-Myc and Klf4 into the somatic genome limits the utility of iPS cells for patient-specific therapy

*Author to whom all correspondence should be addressed.
Email: hiroshi-tomita@iiare.tohoku.ac.jp
Received 28 June 2010; revised 30 November 2010; accepted 30 November 2010.
© 2011 The Authors
Journal compilation © 2011 Japanese Society of Developmental Biologists

(Yamanaka 2007, 2009; Zhou *et al.* 2009). Furthermore, the generation of an iPS cell line takes considerable time (approximately 6 months) and is labor intensive so it can not be generated rapidly (Holden & Vogel 2008).

In the previous studies, most investigators have used undifferentiated cells, such as ES cells, ES cell-derived neural progenitors, bone marrow stromal cells, or iPS cells, as the cell source (Sanchez-Ramos *et al.* 2000; Woodbury *et al.* 2000; Zhao *et al.* 2002; Ikeda *et al.* 2005; Klassen & Reubinoff 2008; Osakada *et al.* 2008; Jin *et al.* 2009). Zhang *et al.* (2010) showed that NIH/3T3 fibroblasts, which are already committed to a specific differentiation destiny, were able to be induced to express neuronal markers, but these cells have to be reprogrammed by adding epigenetic modifiers to make epigenetic modification.

NIH/3T3 fibroblasts, derived from an embryo of the NIH/Swiss mouse, are generally adherently cultured in Dulbecco's modified Eagle's medium (DMEM) supplemented with 10% bovine calf serum, which is the normal culture condition for most investigators. In the present study, we cultured NIH/3T3 cells in a completely different microenvironment to establish whether this cell line could be induced into neuronal cells without adding any epigenetic modifier and to be further induced into retinal photoreceptor-like cells simply by adding taurine and retinoic acid (RA), and we also characterized the mechanism involved.

Materials and methods

Culture of NIH/3T3 fibroblasts

NIH/3T3 fibroblasts were kindly provided by the Cell Resource Center for Biomedical Research, Tohoku University, Japan as a frozen stock. Cells were adherently cultured in DMEM with 10% newborn calf serum (NCS), 1× GlutaMax, and 1× Antibiotic-Antimycotic (Invitrogen/Gibco) on normal tissue culture dishes (uncoated) at 37°C, 5% CO_2, which is referred to as normal conditions (NC).

Generation of neurosphere-like cells (Neurosphere assay)

Neurosphere assays were carried out according to previous studies (Das *et al.* 2006; Brewer & Torricelli 2007) with minimal modifications. Briefly, NIH/3T3 fibroblasts were cultured in suspension in NC or neural stem cell medium (NSCm) on 2.0% agarose-coated dishes at a density of 1×10^5 cells/mL for 5–7 days to detect the ability of these cells to form spheres. NSCm was serum-free and composed of DMEM/F-12, 1× GlutaMax, 1× Antibiotic-Antimycotic, 1× B27 supplement (without vitamin A: Cat. No. 12587), 1× N2 supplement, 20 ng/mL bFGF (basic fibroblast growth factor), and 20 ng/mL EGF (epidermal growth factor). All reagents were obtained from Invitrogen/Gibco. Adherent NIH/3T3 fibroblasts cultured in NC on normal tissue culture dishes were used as a control.

Passage of neurosphere-like cells

After 5–7 days of cultivation, spheres were trypsinized into single cells and resuspended in NSCm. The suspension was plated onto a new 2.0% agarose-coated dish and cultured for another 5–7 days to test the ability of these cells to form secondary spheres.

To examine the proliferative ability and expression of neural progenitor markers of NIH/3T3-derived spheres, after 7 days of floating cultivation for the second passage, the spheres were exposed to 10 μmol/L BrdU (Sigma) to tag the dividing cells and plated onto poly-D-lysine-coated 8-well culture slides (BD Biosciences) for the final 48 h (Das *et al.* 2006). Immunocytochemistry was carried out for double staining analysis of the neural progenitor markers Nestin, Sox2, Pax6, Musashi-1 (Msi1), and BrdU. RNA was isolated from NIH/3T3 cells cultured in different conditions, and real-time polymerase chain reaction (PCR) were performed to compare the expression of neural progenitor markers Nestin and Sox2.

Differentiation of neuron- and glia-like cells

For the differentiating culture, NSCm-cultured spheres were trypsinized into single cells and resuspended in differentiating medium (DM), then plated onto poly-D-lysine-coated 8-well culture slides and cultured for an additional 8 days. In DM, EGF and B-27 supplement (without RA Cat. No.12587) were replaced by 1% serum and standard B-27 supplement (including retinyl acetate: Cat. No. 17504). In addition, brain-derived neurotrophic factor (BDNF: 10 ng/mL) was added to promote the differentiation into neuronal cells, and ciliary neurotrophic factor (CNTF: 20 ng/mL) was added for glial cell differentiation (Yang *et al.* 2005; Das *et al.* 2006; Chen *et al.* 2007; Chojnacki & Weiss 2008; Matsuda *et al.* 2009). Immunocytochemistry was carried out to stain the markers of neurons (β-tubulin and neurofilament 200 [NF200]), astrocytes (glial fibrillary acidic protein [GFAP]), and oligodendrocytes (O4).

Induction of retinal photoreceptor-like cells

For the induction of retinal photoreceptor-like cells, NIH/3T3-derived neuron-like cells were trypsinized and

© 2011 The Authors
Journal compilation © 2011 Japanese Society of Developmental Biologists

resuspended in an induction medium (IM), which is composed of DMEM/F-12 supplemented with 1% NCS, 1× Antibiotic-Antimycotic, 1× Glutamax, 10 ng/mL BDNF and the inducing agent taurine (50 μmol/L) plus RA (10 μmol/L), then plated onto poly-D-lysine-coated 8-well culture slides to culture for an additional 8 days (Das *et al.* 2006; Osakada *et al.* 2008). Cells were fixed and immunocytochemistry was performed by staining the retinal photoreceptor markers rhodopsin and recoverin.

Real-time PCR

Real-time PCR was performed as previously described (Sugano *et al.* 2003). Total RNA was isolated from cultured cells using Trizol (Sigma). cDNA synthesis was carried out using the First-Strand cDNA Synthesis kit (GE Healthcare). SYBR Premix Ex Taq (Perfect Real Time; Takara) was used for PCR reactions. Specific transcripts were amplified on a Smart Cycler (Takara) for 35–40 cycles. The expression level of each gene was calculated by normalizing it with the glyceraldehyde 3-phosphate dehydrogenase (GAPDH) gene (TaqMan Rodent GAPDH Control Reagents; Applied Biosystems). The primers used in the experiment are shown in Table 1.

Immunocytochemical analysis

Immunocytochemistry was performed by staining cell-specific markers as previously described (Sugano *et al.* 2005; Das *et al.* 2006). Briefly, cells were fixed with 4% paraformaldehyde for 10 min at room temperature. After permeabilization with 0.3% Triton X-100 in phosphate-buffered saline (PBS) for 10 min, slides were incubated in 1% bovine serum albumin (BSA) and 5% blocking serum for 30 min at room temperature. Primary antibodies were added and incubated overnight at 4°C. The list of antibodies and their dilution are given in Table 2. Slides were washed and incubated with the secondary antibodies conjugated to Alexa Fluor 594 (red) or Alexa Fluor 488 (green) (Invitrogen-Molecular Probes) in the dark for 30 min at room temperature. A negative control was performed by replacing the primary antibody with normal IgG. For staining of nuclei, cells were covered with Vectashield medium including 4′6′-diamidino-2-phenylindole dihydrochloride (DAPI) (Vector Laboratories Inc.). Fluorescence was excited and labeled cells were imaged with a fluorescence microscope (Axiovert40; Zeiss, Germany).

Protein extraction and western blotting

Western blotting analysis was performed as previously described (Takahashi & Yamanaka 2006). Briefly, the NIH/3T3 cells were lysed with RIPA buffer supplemented with cocktail (Roche), and cell lysates (50 μg) were separated by electrophoresis on Mini-PROTEAN TGX gel (BIO-RAD) and transferred to an immuno-blot PVDF membrane (BIO-RAD). Antibodies used were Sox2, Nestin (1:200, shown in Table 2), anti-rabbit and anti-mouse IgG (H&L) AP conjugate (1: 7500, Promega).

Statistical analysis

The data of real-time PCR analysis are expressed as mean ± SD. Significance between groups was analyzed by one-way analysis of variance (ANOVA) with GraphPad Prism 4.0 software (San Diego). Values of $P < 0.05$ were considered statistically significant.

Results

NIH/3T3 fibroblasts can form neurosphere-like cells in defined conditions

First, we carried out a neurosphere assay on floating NIH/3T3 cells cultured in two different proliferating media: NSCm and NC. When NIH/3T3 cells were cultured in suspension for 2–5 days, NIH/3T3 cells formed spheres (Fig. 1B,C), which displayed classic features of neurospheres, in both proliferating media. There was no apparent difference in morphology between NC- and NSCm-cultured spheres for the first 2–3 days of culture. All NSCm-cultured spheres had a regular and round shape with bright borders on the edge of spheres (Fig. 1B). However, after 4–5 days of culture, the diameter of NC-cultured spheres did not increase, and some of these spheres showed an irregular and unhealthy appearance with dark or indistinct borders (Fig. 1C), which was assumed to be

Table 1. Sequences of primers used in real-time polymerase chain reaction (PCR)

Gene	Primer sequence (5′-3′) F	R	Product (bp)	Annealing temp. (°C)	GeneBank accession number
Nestin	AGACAGTGAGGCAGATGAGT	ATGAGAGGTCAGAGTCATGG	224	55	NM_016701
Sox2†	TAGAGCTAGACTCCGGGCGATGA	TTGCCTTAAACAAGACCACGAAA	296	60	NM_011443

†Primers of Sox2 were from Takahashi & Yamanaka (2006).

© 2011 The Authors
Journal compilation © 2011 Japanese Society of Developmental Biologists

Table 2. List of antibodies used to stain different target cells

Antibody	Species	Dilution	Company and catalog no.	Target cells
Nestin	Mouse	1:500	Millipore-Chemicon:MAB353	Neural progenitors
Sox2	Rabbit	1:100	Santa Cruz Biotechnology, Inc: sc-20088	Neural progenitors
Msi1	Rabbit	1:100	Sigma-Aldrich: M3571	Neural progenitors
Pax6	Rabbit	1:100	Santa Cruz Biotechnology, Inc: sc-32766	Neural progenitors
BrdU	Mouse	1:100	Santa Cruz Biotechnology, Inc: sc-32323	Proliferating cells
β-tubulin	Mouse	1:500	Sigma: T5076	Neurons
NF200	Mouse	1:100	Sigma: N0142	Neurons
GFAP	Goat	1:100	Santa Cruz Biotechnology, Inc: sc-6171	Astrocytes
O4	Mouse	1:100	Chemicon International, Inc.: MAB345	Oligodendrocytes
Rhodopsin	Mouse	1:100	Millipore-Chemicon: MAB5316	Photoreceptors
Recoverin	Goat	1:100	Santa Cruz Biotechnology, Inc: sc-20353	Photoreceptors

BrdU, 5-Bromo-2′-deoxyuridine; GFAP, glial fibrillary acicic protein; Msi1, Musashi homologue 1; NF200, neurofilament 200 kDa; O4, oligodendrocyte marker O4; Pax6, paired box protein 6; Sox2, SRY (sex determining region Y)-box containing gene 2.

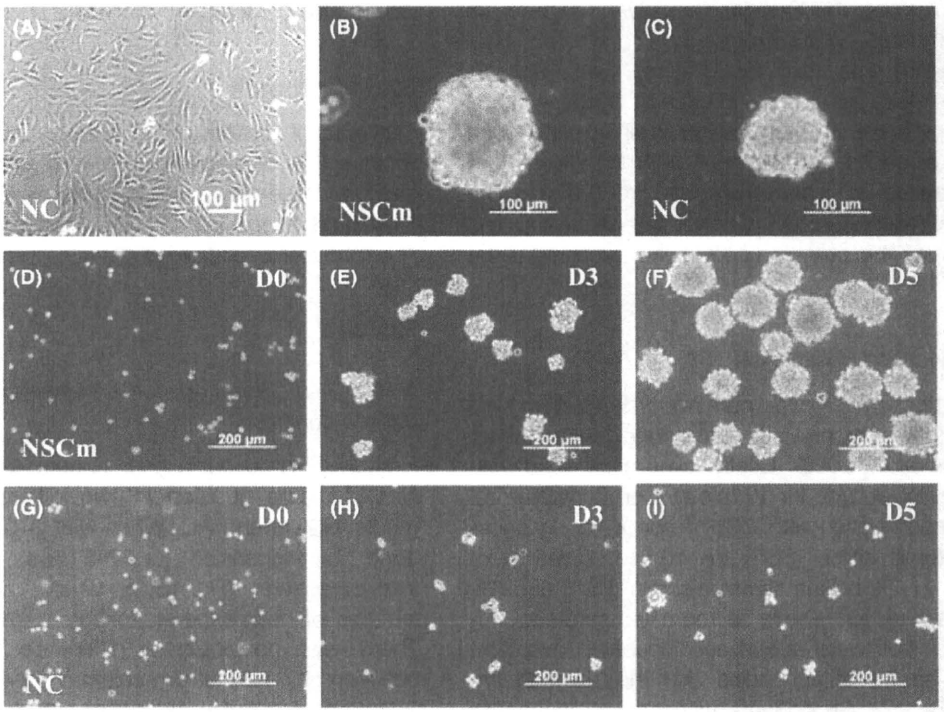

Fig. 1. Generation and passage of NIH/3T3-derived neurosphere-like cells. NIH/3T3 fibroblasts were adherently cultured in normal condition (NC) on normal (uncoated) dishes (A). Spheres were generated after culturing in neural stem cell medium (NSCm) (B) or NC (C) on 2% agarose-coated dishes for 5 days. Generation of the secondary spheres were carried out by culturing in NSCm (D–F) or NC (G–I) for 0, 3, and 5 days. The NSCm-cultured secondary spheres were observed on day 3 (E) after passaging, and the diameter had doubled by day 5 (F). NC-cultured spheres formed very small secondary spheres, and the diameter was unchanged after 3–5 days of culture (H and I).

surrounded by many dying cells caused by the lack of necessary growth factors.

Second, we tested the ability of NIH/3T3-derived spheres to generate secondary spheres. After dissociating into single cells and culturing for 3–7 days, the secondary spheres were quickly formed (on days 3–5) in NSCm, and the sphere size was dependent on culture time with defined cell density (Fig. 1D–F). These cells could generate sub-spheres for an extended period of three passages (more passages were untested). However, NC-cultured spheres formed only very small secondary spheres on days 3–5 after passaging (Fig. 1G–I), and tertiary spheres were difficult to generate.

© 2011 The Authors
Journal compilation © 2011 Japanese Society of Developmental Biologists

NIH/3T3-derived spheres express neural progenitor markers

Third, we performed immunocytochemistry to stain the neural progenitor markers Nestin, Sox2, Pax6, and Msi1 for NSCm-cultured NIH/3T3-derived spheres, and the results showed that these cells expressed neural progenitor markers (Fig. 2E–T). Some of these spheres co-expressed Nestin and Sox2 (Fig. 2J–L), suggesting that some cells expressed multiple neural progenitor markers. Double staining for Sox2, Pax6, and Msi1 with BrdU indicated that these spheres were composed of dividing cells that entered the cell cycle (Fig. 2N–P,R,T).

To compare the neural progenitor potential of NIH/3T3 cells cultured in different conditions, the expression of neural progenitor markers Sox2 and Nestin were examined by real-time PCR. Sox2 (Fig. 2V) and Nestin (Fig. 2W) were significantly upregulated in NSCm-cultured spheres compared with adherent NIH/3T3 fibroblasts or NC-cultured spheres. Moreover, the expression of Nestin and Sox2 were also observed from NSCm-cultured spheres by western blotting (Fig. 2X).

NIH/3T3-derived spheres have the potential to differentiate into neuronal cells

Subsequently, we tested whether NIH/3T3-derived spheres can be differentiating into neuronal cells. After transferring to the DM, these spheres were cultured for another 8 days. Immunocytochemical results showed that these cells expressed the neuronal markers β-tubulin (Fig. 3D) and NF200 (Fig. 3H) and the astrocytic marker GFAP (Fig. 3K), although expression of GFAP was very low. However, these cells did not express the oligodendrocyte marker O4 (data not shown).

NIH/3T3-derived spheres can be induced to express retinal photoreceptor markers

Finally, to determine the ability of NIH/3T3 cells to differentiate along neural lineage, we treated NIH/3T3-derived neuron-like cells with taurine and RA, both of which show effective promotion of neuron induction. After treatment with these chemicals, expression of the neuronal marker β-tubulin (Fig. 4E) was greatly enhanced, and expression of photoreceptor markers rhodopsin (Fig. 4I,K,M) and recoverin (Fig. 4L,M) was also induced. Double staining results showed that some cells co-expressed recoverin and rhodospin (Fig. 4K–M); however, the expression of recoverin was very low (Fig. 4L–N). Real-time PCR analysis showed that neural progenitor markers Sox2 and Nestin were significantly downregulated during the differentiation and induction of neuron- and photoreceptor-like cells (Fig. 4O,P).

Discussion

Many studies have shown that the undifferentiated cells, such as ES cells, ES-derived neural stem cells (NSCs), bone marrow stromal cells or iPS cells have the ability to be differentiated along the neuronal lineage (Sanchez-Ramos *et al.* 2000; Woodbury *et al.* 2000; Zhao *et al.* 2002; Ikeda *et al.* 2005; Takahashi & Yamanaka 2006; Osakada *et al.* 2008, 2009; Hirami *et al.* 2009; Jin *et al.* 2009) and could be potential targets for the replacement therapy for retinal degeneration diseases. However, the ability of differentiated cells to be transdifferentiated into neuronal cells has not been widely investigated. Zhang *et al.* (2010) showed that the NIH/3T3 fibroblasts were able to be induced to express neuronal markers after the epigenetic modification by adding epigenetic modifiers, but the question of whether the differentiated cells could be transdifferentiated into neuronal cells without adding any epigenetic modifier and the mechanism involved still remain to be characterized.

Our study showed that NIH/3T3 fibroblasts were able to form spheres composed of dividing cells in suspension culture in the presence of EGF, bFGF and B27 supplement (without vitamin A), which are conditions suitable for the proliferation of neural progenitors. These spheres were able to be serially passaged to form more sub-spheres, and these cells were incorporated with BrdU, indicating their ability to self-renew. NSCm-cultured spheres express neural progenitor markers Nestin, Sox2, Pax6 and Msi1, indicating that these cells may have the potential to proliferate toward neural progenitor lineage. NIH/3T3-derived spheres was able to be differentiated into both neuronal and astrocytic cell types by removing EGF and B27 supplement (without vitamin A) from the medium and substituting them with serum, standard B-27 supplement and BDNF or CNTF, and also have the potential to be induced into photoreceptor-like cells. Taken together, these results suggested that NIH/3T3-derived neurosphere-like cells can undergo self-renewal and differentiation into neuron-like cells without any epigenetic modification, which are properties of neural progenitors, suggesting the possible neuronal lineage of NIH/3T3 fibroblasts.

To test whether the NIH/3T3-derived spheres obtained were neurospheres or neural progenitors, three functional attributes that define neural progenitors (or neural stem cells) must be exhibited. The first

© 2011 The Authors
Journal compilation © 2011 Japanese Society of Developmental Biologists

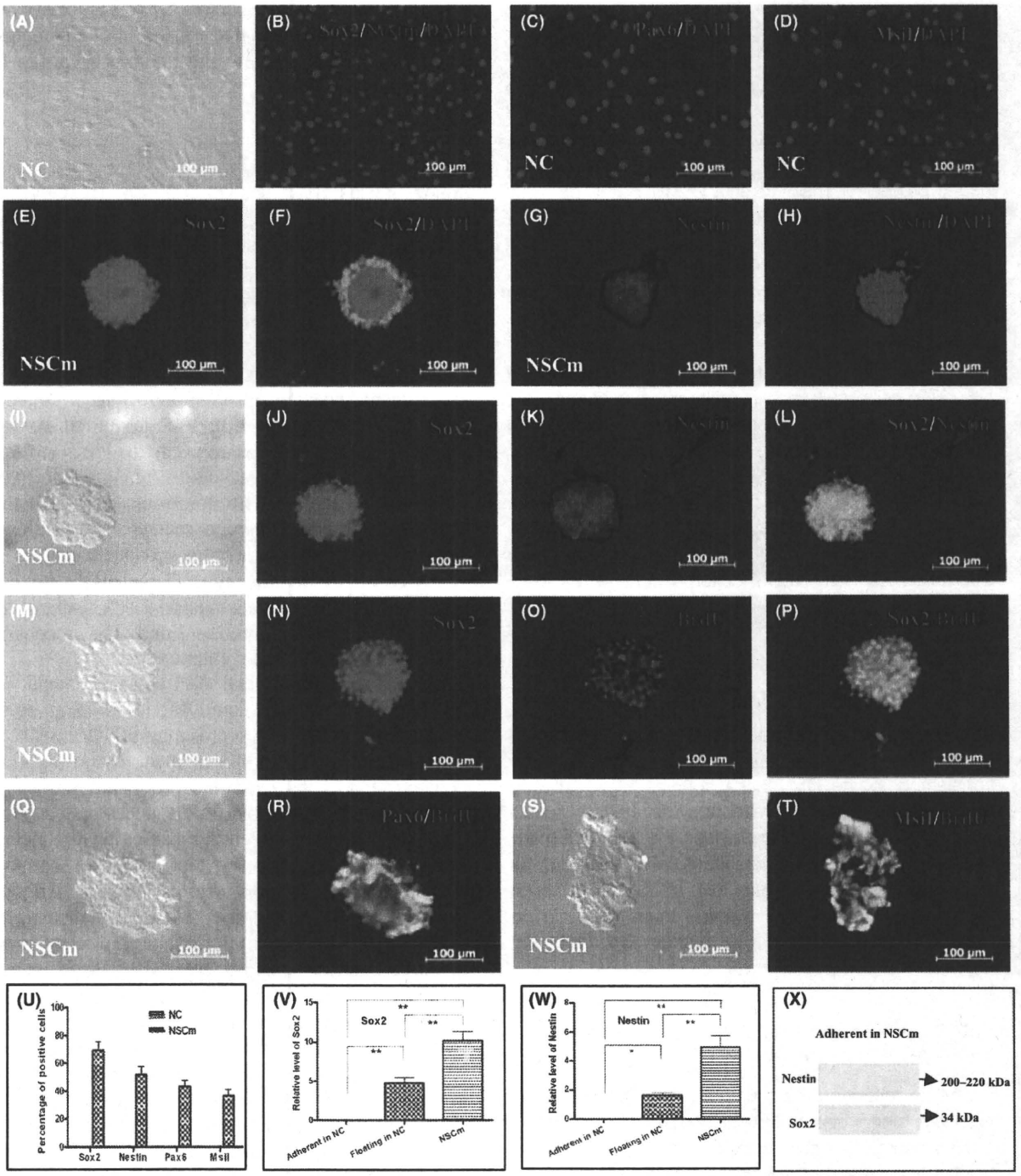

Fig. 2. Neural stem cell medium (NSCm)-cultured NIH/3T3-derived neurosphere-like cells expressed neural progenitor markers. NC-cultured NIH/3T3 fibroblasts did not express any neural progenitor marker (B–D). Single and double staining of Sox2 (E, F, J and L) and Nestin (G, H, K and L) demonstrated that these spheres co-expressed multiple neural progenitor markers. Some spheres were positively stained with BrdU and Sox2 (N-P), Pax-6 (R), Msi1 (T), indicating their proliferative property. Phase contrast images of NIH/3T3 cells cultured in NC (A) and NSCm (I, M, Q and S) were also shown. The percentage of positive cells is presented in the graph (U). Real-time PCR analysis of Sox2 (V) and Nestin (W) were performed for NIH/3T3 cells adherent in NC, floating in NC or NSCm. The columns represent the relative expression level of Sox2 or Nestin in spheres compared with those of adherent NIH/3T3 fibroblasts. Western blotting analysis of Sox2 and Nestin in NC- and NSCm-cultured NIH/3T3 cells were shown in X. The symbols * and ** represent $P < 0.05$ and $P < 0.01$, respectively.

© 2011 The Authors
Journal compilation © 2011 Japanese Society of Developmental Biologists

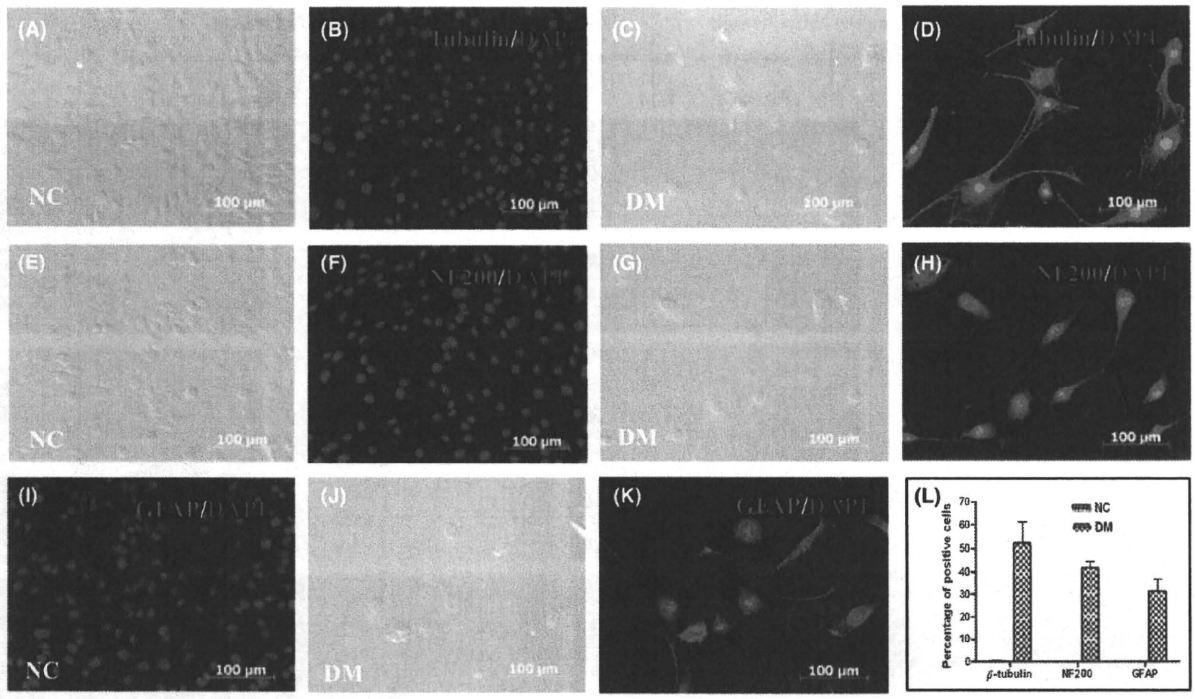

Fig. 3. Differentiation of neural stem cell medium (NSCm)-cultured NIH/3T3-derived neurosphere-like cells into neuron- and astrocyte-like cells. When shifted to DM, these cells expressed markers corresponding to neurons (β-tubulin [D] and NF200 [H]) and astrocytes (glial fibrillary acidic protein [GFAP] [K]). NIH/3T3 fibroblasts cultured in normal conditions (NC) were used as a control (A, B, E, F, and I). Phase contrast images of NIH/3T3 cells cultured in NC (A and E) and DM (C, G and J) were also shown. The percentage of positive cells expressing neuronal or glial markers is presented in the graph (L).

property is self-renewal wherein cells from spheres proliferate and make identical copies of themselves. The second is multipotency, wherein the spheres are able to generate all three main cell lineages of the mammalian central nervous system (CNS), neurons, astrocytes, and oligodendrocytes. The third is the ability to generate tissues. The generation of a neurosphere even from a particular region of the CNS does not necessarily denote to be neural progenitors unless there is supporting *in vivo* evidence (Chojnacki & Weiss 2008; Ahmed 2009). This neurosphere protocol has been used in a number of studies to examine the properties of various progenitors (Chaichana *et al.* 2006; Das *et al.* 2006; Jensen & Parmar 2006; Marshall *et al.* 2006; Chojnacki & Weiss 2008).

In the present study, we demonstrated the self-renewal property of NIH/3T3-derived spheres, and we also showed the potential of these cells to differentiate along two basic CNS lineages, neurons and astrocytes; however, we failed to show the expression of the oligodendrocyte marker O4.

These results predicted two possibilities. One is that these NIH/3T3-derived spheres are not neural progenitors, but only some NIH/3T3 cells with changes in morphology and properties. Because the growth of cells *in vivo* and *in vitro* are tightly regulated by their microenvironments (Hegde *et al.* 2007), NIH/3T3 fibroblasts are likely to survive in NSCm, display classic morphology of neurospheres and respond to growth factor exposure in a similar manner that was exhibited by neural progenitors. For example, the markers of neural progenitors were upregulated and some cells had the potential to differentiate toward neural lineage. However, most of these cells still preserved the property of NIH/3T3 fibroblasts, and could not be differentiated into all three main types of CNS lineages.

The other possibility is that these NIH/3T3-derived spheres may be immature neural progenitors. These spheres could proliferate, express markers of neural progenitors and generate neuron and astrocyte markers. The reason why these spheres did not express the oligodendrocyte marker O4 may be due to the lack of some growth factor(s) in the differentiating medium or the shortage of culture period, which may be critical for the generation of oligodendrocyte progenitors or oligodendrocytes. The cytokine CNTF alone might not be sufficient for the generation of oligodendrocytes, further investigations are needed to detect whether oligodendrocytes can be generated by adding other candidate factor(s), for example, platelet-derived

© 2011 The Authors
Journal compilation © 2011 Japanese Society of Developmental Biologists

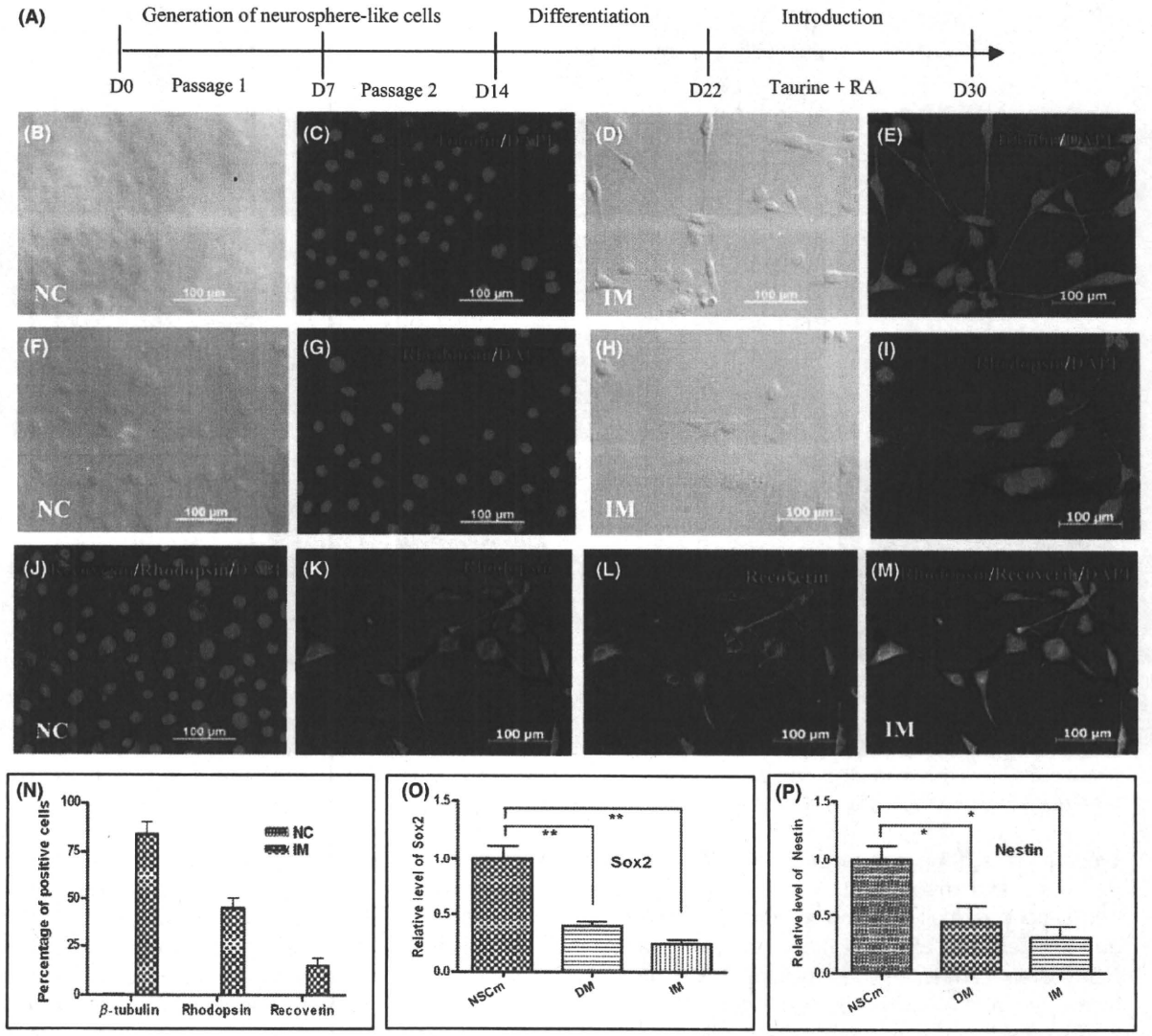

Fig. 4. Induction of neuron- and photoreceptor-like cells by treating cells with the combination of 50 μmol/L taurine and 10 μmol/L retinoic acid (RA). (A). Procedure for induction of retinal photoreceptor-like cells from NIH/3T3 fibroblasts. Immunocytochemical analysis of β-tubulin (C and E), rhodopsin (G, I, J, K and M) and recoverin (J, L and M) was performed for the treated (E, I, and K-M) and untreated (C, G and J) cells. Phase contrast images of NIH/3T3 cells cultured in NC (B and F) and IM (D and H) were also shown. The percentage of positive cells expressing neuronal or photoreceptor markers is presented in the graph (N). Real-time PCR was carried out to analyze Sox2 (O) and Nestin (P) expression in NSCm-, DM- and IM-cultured cells. The symbols * and ** represent $P < 0.05$ and $P < 0.01$, respectively.

growth factor AA, which was demonstrated to effectively enhance survival of oligodendrocyte progenitors (Yang *et al.* 2005; Chen *et al.* 2007).

Our study demonstrates that NIH/3T3 fibroblasts display some features of neural progenitors and express neuron, astrocyte and even photoreceptor markers under defined conditions. These results shed some light on the induction of retinal photoreceptors from a differentiated cell source. Further studies are necessary to determine if NIH/3T3 fibroblasts can be differentiated into functional neurons or photoreceptors, but the present study suggests that neuronal cells can be generated from differentiated cells of other types without the need of adding any epigenetic modifier.

Acknowledgments

This work was supported in part by the Ministry of Health, Labour and Welfare, Japan Foundation for Aging and Health and the Program for Promotion of Fundamental studies in Health Sciences of the National Institute of Biomedical Innovation (NIBIO).

© 2011 The Authors
Journal compilation © 2011 Japanese Society of Developmental Biologists

References

Ahmed, S. 2009. The culture of neural stem cells. *J. Cell. Biochem.* **106**, 1–6.

Brewer, G. J. & Torricelli, J. R. 2007. Isolation and culture of adult neurons and neurospheres. *Nat. Protoc.* **2**, 1490–1498.

Chaichana, K., Zamora-Berridi, G., Camara-Quintana, J. & Quinones-Hinojosa, A. 2006. Neurosphere assays: growth factors and hormone differences in tumor and nontumor studies. *Stem cells* **24**, 2851–2857.

Chen, Y., Balasubramaniyan, V., Peng, J., Hurlock, E. C., Tallquist, M., Li, J. & Lu, Q. R. 2007. Isolation and culture of rat and mouse oligodendrocyte precursor cells. *Nat. Protoc.* **2**, 1044–1051.

Chojnacki, A. & Weiss, S. 2008. Production of neurons, astrocytes and oligodendrocytes from mammalian CNS stem cells. *Nat. Protoc.* **3**, 935–940.

Das, A. V., Mallya, K. B., Zhao, X., Ahmad, F., Bhattacharya, S., Thoreson, W. B., Hegde, G. V. & Ahmad, I. 2006. Neural stem cell properties of Müller glia in the mammalian retina: regulation by Notch and Wnt signaling. *Dev. Biol.* **299**, 283–302.

Hegde, G. V., James, J., Das, A. V., Zhao, X., Bhattacharya, S. & Ahmad, I. 2007. Characterization of early retinal progenitor microenvironment: presence of activities selective for the differentiation of retinal ganglion cells and maintenance of progenitors. *Exp. Eye Res.* **84**, 577–590.

Hirami, Y., Osakada, F., Takahashi, K., Okita, K., Yamanaka, S., Ikeda, H., Yoshimura, N. & Takahashi, M. 2009. Generation of retinal cells from mouse and human induced pluripotent stem cells. *Neurosci. Lett.* **458**, 126–131.

Hoffman, L. M. & Carpenter, M. K. 2005. Characterization and culture of human embryonic stem cells. *Nat. Biotechnol.* **23**, 699–708.

Holden, C. & Vogel, G. 2008. A seismic shift for stem cell research. *Science* **319**, 560–563.

Ikeda, H., Osakada, F., Watanabe, K., Mizuseki, K., Haraguchi, T., Miyoshi, H., Kamiya, D., Honda, Y., Sasai, N., Yoshimura, N., Takahashi, M. & Sasai, Y. 2005. Generation of Rx+/Pax6 + neural retinal precursors from embryonic stem cells. *Proc. Natl Acad. Sci. USA* **102**, 11331–11336.

Jensen, J. B. & Parmar, M. 2006. Strengths and limitations of the neurosphere culture system. *Mol. Neurobiol.* **34**, 153–161.

Jin, W., Xing, Y. Q. & Yang, A. H. 2009. Epidermal growth factor promotes the differentiation of stem cells derived from human umbilical cord blood into neuron-like cells via taurine induction in vitro. *In Vitro Cell. Dev. Biol. Anim.* **45**, 321–327.

Klassen, H. & Reubinoff, B. 2008. Stem cells in a new light. *Nat. Biotechnol.* **26**, 187–188.

Marshall, G. P., Reynolds, B. A. & Laywell, E. D. 2006. Using the neurosphere assay to quantify neural stem cells in vivo. *Curr. Pharm. Biotechnol.* **8**, 141–145.

Matsuda, N., Lu, H., Fukata, Y., Noritake, J., Gao, H. F., Mukherjee, S., Nemoto, T., Fukata, M. & Poo, M. M. 2009. Differential activity-dependent secretion of brain-derived neurotrophic factor from axon and dendrite. *J. Neurosci.* **29**, 14185–14194.

Osakada, F., Ikeda, H., Sasai, Y. & Takahashi, M. 2009. Stepwise differentiation of pluripotent stem cells into retinal cells. *Nat. Protoc.* **4**, 811–824.

Osakada, F., Ikeda, H., Mandai, M., Wataya, T., Watanabe, K., Yoshimura, N., Akaike, A., Sasai, Y. & Takahashi, M. 2008. Toward the generation of rod and cone photoreceptors from mouse, monkey and human embryonic stem cells. *Nat. Biotechnol.* **26**, 215–222.

Sanchez-Ramos, J., Song, S., Cardozo-Pelaez, F., Hazzi, C., Stedeford, T., Willing, A., Freeman, T. B., Saporta, S., Janssen, W., Patel, N., Cooper, D. R. & Sanberg, P. R. 2000. Adult bone marrow stromal cells differentiate into neural cells in vitro. *Exp. Neurol.* **164**, 247–256.

Sugano, E., Tomita, H., Abe, T., Yamashita, A. & Tamai, M. 2003. Comparative study of cathepsins D and S in rat IPE and RPE cells. *Exp. Eye Res.* **77**, 203–209.

Sugano, E., Tomita, H., Ishiguro, S., Abe, T. & Tamai, M. 2005. Establishment of effective methods for transducing genes into iris pigment epithelial cells by using adeno-associated virus type 2. *Invest. Ophthalmol. Vis. Sci.* **46**, 3341–3348.

Takahashi, K. & Yamanaka, S. 2006. Induction of pluripotent stem cells from mouse embryonic and adult fibroblast cultures by defined factors. *Cell* **126**, 663–676.

Woodbury, D., Schwarz, E. J., Prockop, D. J. & Black, I. B. 2000. Adult rat and human bone marrow stromal cells differentiate into neurons. *J. Neurosci. Res.* **61**, 364–370.

Yamanaka, S. 2007. Strategies and new developments in the generation of patient-specific pluripotent stem cells. *Cell Stem Cell* **1**, 39–49.

Yamanaka, S. 2009. A fresh look at iPS cells. *Cell* **137**, 13–17.

Yang, Z. S., Watanabe, M. & Nishiyama, A. 2005. Optimization of oligodendrocyte progenitor cell culture method for enhanced survival. *J. Neurosci. Methods* **149**, 50–56.

Zhang, X. M., Li, Q. M., Su, D. J., Wang, N., Shan, Z. Y., Jin, L. H. & Lei, L. 2010. RA induces the neural-like cells generated from epigenetic modified NIH/3T3 cells. *Mol. Biol. Rep.* **37**, 1197–1202.

Zhao, X., Liu, J. N. & Ahmad, I. 2002. Differentiation of embryonic stem cells into retinal neurons. *Biochem. Biophys. Res. Commun.* **297**, 177–184.

Zhou, H., Wu, S., Joo, J. Y., Zhu, S., Han, D. W., Lin, T., Trauger, S., Bien, G., Yao, S., Zhu, Y., Siuzdak, G., Schöler, H. R., Duan, L. & Ding, S. 2009. Generation of induced pluripotent stem cells using recombinant proteins. *Cell Stem Cell* **4**, 381–384.

© 2011 The Authors
Journal compilation © 2011 Japanese Society of Developmental Biologists

Gene Therapy (2010), 1–9
© 2010 Macmillan Publishers Limited All rights reserved 0969-7128/10
www.nature.com/gt

ORIGINAL ARTICLE

Immune responses to adeno-associated virus type 2 encoding channelrhodopsin-2 in a genetically blind rat model for gene therapy

E Sugano[1], H Isago[1], Z Wang[1,2], N Murayama[1], M Tamai[3] and H Tomita[1,4,5]

We had previously reported that transduction of the channelrhodopsin-2 (ChR2) gene into retinal ganglion cells restores visual function in genetically blind, dystrophic Royal College of Surgeons (RCS) rats. In this study, we attempted to reveal the safety and influence of exogenous ChR2 gene expression. Adeno-associated virus (AAV) type 2 encoding ChR2 fused to Venus (rAAV-ChR2V) was administered by intra-vitreous injection to dystrophic RCS rats. However, rAAV-ChR2 gene expression was detected in non-target organs (intestine, lung and heart) in some cases. ChR2 function, monitored by recording visually evoked potentials, was stable across the observation period (64 weeks). No change in retinal histology and no inflammatory marker of leucocyte adhesion in the retinal vasculature were observed. Although antibodies to rAAV (0.01–12.21 $\mu g\,ml^{-1}$) and ChR2 (0–4.77 $\mu g\,ml^{-1}$) were detected, their levels were too low for rejection. T-lymphocyte analysis revealed recognition by T cells and a transient inflammation-like immune reaction only until 1 month after the rAAV-ChR2V injection. In conclusion, ChR2, which originates from *Chlamydomonas reinhardtii*, can be expressed without immunologically harmful reactions *in vivo*. These findings will help studies of ChR2 gene transfer to restore vision in progressed retinitis pigmentosa.
Gene Therapy advance online publication, 28 October 2010; doi:10.1038/gt.2010.140

Keywords: retinitis pigmentosa; channelrhodopsin-2; immunoreactivity; adeno-associated virus; retinal ganglion cells

INTRODUCTION

Retinitis pigmentosa (RP) is a group of diseases in which a gene mutation results in the death of photoreceptor cells. At present, approximately 40 genes have been identified as the causative agents (http://www.sph.uth.tmc.edu/retnet/; provided in the public domain by the University of Texas Houston Health Science Center, Houston, TX, USA). The initial visual impairment in patients with RP is night blindness, and patients lose their vision in the final stage of this disease following visual field loss.[1] Many trials have been conducted to identify agents that can protect photoreceptors and delay vision loss, but effective treatments have not been developed against progressed RP.

Although photoreceptor cells are often degenerated in the case of progressed RP, other inner neurons, including retinal ganglion cells (RGCs) are preserved.[2] It would be ideal to utilise the remaining retinal neurons to restore vision. We have been studying light-gated cation-selective membrane channel protein channelrhodopsin-2 (ChR2)[3] to induce photoreceptor function in retinal neurons such as RGCs[4,5] and ON bipolar cells.[6] We have already demonstrated that the responses induced by various stimulus frequencies (Hz) in ChR2-transduced rats are in no way inferior to those in normal rats,[7] as supported by the finding that ChR2-induced photocurrents are extremely fast.[8,9] Visual function was also well analysed by using transgenic rats with ChR2 transduction into RGCs: the spatial frequencies based on behavioural responses of photoreceptor-degenerated ChR2 transgenic rats were the same as those of normal rats.[10] These studies indicate that transfer of the ChR2 gene into the remaining retinal neurons is a useful method for restoring vision in progressed RP.

However, for clinical application of ChR2 therapy, some problems must be considered. First, this approach is a gene therapy. An immune response (mostly a problem with adenovirus- and herpes simplex virus-derived vectors)[11] may be caused by adeno-associated virus (AAV) and its incorporation into the host genome may lead to de-repression of tumour suppression genes.[12–14] Second, ChR2 is a protein originating from *Chlamydomonas reinhardtii*. It is important to study the systemic responses on virus vector application and long-term expression of the transgene product in humans. In this study, to reveal the safety and influence of exogenous ChR2 gene expression, we investigated the functional stability of the ChR2 gene and the possibility of harmful immune reactions caused by this gene therapy in a Royal College of Surgeons (RCS) rat model of RP.

RESULTS

Recording of visually evoked potentials (VEPs) in RCS rats

Although RGCs are maintained in aged RCS (*rdy/rdy*) rats, VEPs would be abolished because of the loss of light-evoked synchronous activities by photoreceptor cells. Indeed, VEPs were not evoked even

[1]Department of International Advanced Interdisciplinary Research, Institute for International Advanced Research and Education, Tohoku University, Sendai, Japan; [2]Japan Foundation for Aging and Health, Aichi, Japan; [3]School of Medicine, Tohoku University, Sendai, Japan; [4]United Centers for Advanced Research and Translational Medicine, School of Medicine, Tohoku University, Sendai, Japan and [5]Innovation of New Biomedical Engineering Center, Tohoku University, Sendai, Japan
Correspondence: Dr H Tomita, Department of International Advanced Interdisciplinary Research, Institute for International Advanced Research and Education, Tohoku University, 4-1 Seiryo-machi, Aoba-ku, Sendai 980-8575, Japan.
E-mail: hiroshi-tomita@iiare.tohoku.ac.jp
Received 9 June 2010; revised 29 August 2010; accepted 7 September 2010

by the maximum flash of the light-emitting diode in any of the 6-month-old RCS (*ryd/rdy*) rats. After confirmation of the loss of photoreceptor-derived function, AAV encoding ChR2 fused to Venus (rAAV-ChR2V) was administered by intra-vitreous injection into the left eye. The right eye was not treated and served as the control. At 2 weeks after the injection, VEPs were recorded in the right visual cortex. The amplitude peaked at 8 weeks but remained stable until 64 weeks after the injection (Figure 1). There was no recording from the left side of the visual cortex (data not shown). We could not record for longer periods than 64 weeks because the lifespan of RCS rats is about 2 years.

Viral dissemination to the organs

To determine systemic dissemination of rAAV after the injection, total ribonucleic acids were isolated from each organ after 6 months of rAAV-ChR2V administration. No rAAV-derived Venus expression was detected by reverse transcription-polymerase chain reaction (RT-PCR) analysis from the brain, liver, spleen and kidney (Figure 2). As expected, we detected the appropriate Venus protein expression from the rAAV-transduced retinas. Venus expression was unexpectedly detected in other organs (heart, lung and intestine) in some cases.

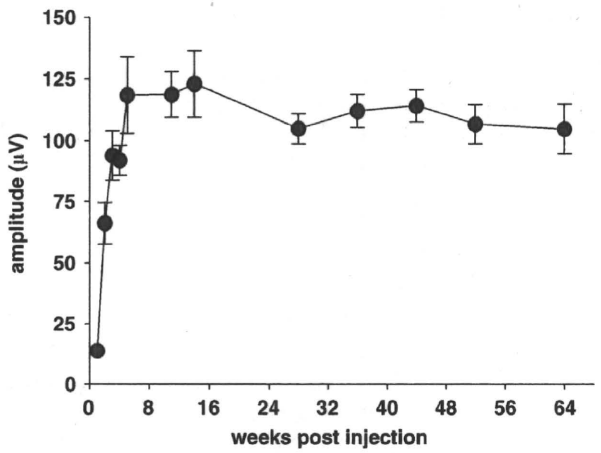

Figure 1 Long-term functional analysis of photosensitivity following ChR2 gene transfer by intra-vitreous injection of rAAV-ChR2V in 6-month-old RCS (*rdy/rdy*) rats. A blue LED (wavelength, 435–500 nm; peak, 470 nm) was flashed for 20 ms at 2.6 mW cm^{-2} and time-dependent improvements in the amplitude of the VEPs were recorded. After peaking at 8 weeks of administration, the amplitude remained stable for 64 weeks post-injection.

Histological examination of rAAV-ChR2V-treated retina

The rAAV-derived gene expression was investigated by observing whole-mounted retina. At 6 months after rAAV administration, the expression of ChR2V or Venus was observed by fluorescence microscopy (Figure 3). ChR2V was expressed in the plasma membrane of the retinal cells; on the other hand, Venus expression was observed in the cytoplasm of the rAAV-Venus-injected retina. Both of the rAAV-derived proteins were expressed all over the retina, and there was some deflection of the retinal expression.

To assess the side effects of ChR2 gene transfer by using rAAV, histological studies were performed on paraffin-embedded and frozen sections. There was no obvious difference in the retinal morphology between the ChR2-injected and the age-matched untreated RCS (*rdy/rdy*) rats (Figures 4a and b). However, intra-vitreous injection of lipopolysaccharide, which resulted in endotoxin-induced uveitis (EIU), in the RCS (+/+) rats caused substantial migration of inflammatory cells, mainly polymorphonuclear leucocytes, in the neural retina and vitreous humour (Figure 4d).

When the retinal activities were studied in frozen sections by immunohistochemistry (Figure 5), glial fibrillary acidic protein (GFAP) expression was restricted to the ganglion cell layers in the rAAV-ChR2V-treated retina (Figure 5c); however, GFAP expression was observed throughout the inner half of the retina in the untreated RCS (Figure 5b) and rAAV-Venus-injected RCS (Figure 5d) rats. Nuclear factor-κB (NF-κB) expression was restricted to the ganglion cell layers in all the tested RCS rats, but it was markedly high in the rAAV-ChR2V-treated retinas (Figure 5h).

Effects of rAAV-ChR2V treatment on leucocyte adhesion in the retinal vasculature

The retinal adherent leucocytes were imaged by perfusion labelling with fluorescein isothiocyanate-coupled concanavalin A. According to a report of Koizumi *et al.*,[15] leucocyte adhesion is significantly elevated

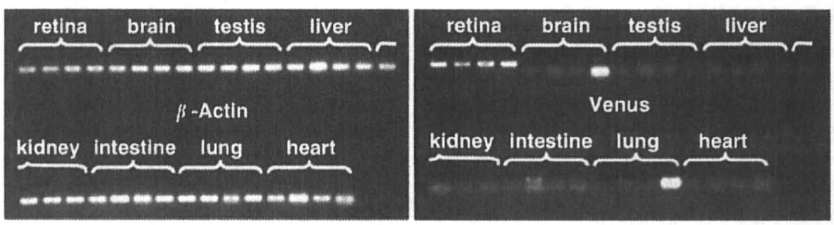

The expression of venus protein, which was carried by rAAV

	retina	brain	testis	liver	kidney	intestine	lung	heart
Sample1	+++	-	-	-	-	-	-	-
Sample2	+++	-	-	-	-	++	-	+
Sample3	+++	-	-	-	-	-	-	+
Sample4	+++	-	-	-	-	-	+	+

Abbreviations : -, No expression; +, Light expression; + + , Moderate expression; + + + , Intense expression;

Figure 2 Virus dissemination to the organs. At 6 months after the administration of rAAV-ChR2V, total ribonucleic acid was extracted from the retina, brain, testis, liver, kidney, intestine, lung and heart. The rAAV-derived gene was investigated by using RT-PCR analysis. As expected, a high copy number of the rAAV-derived gene expression was detected in the retina. The gene expression was also detected in the heart, lung and intestine in some cases.

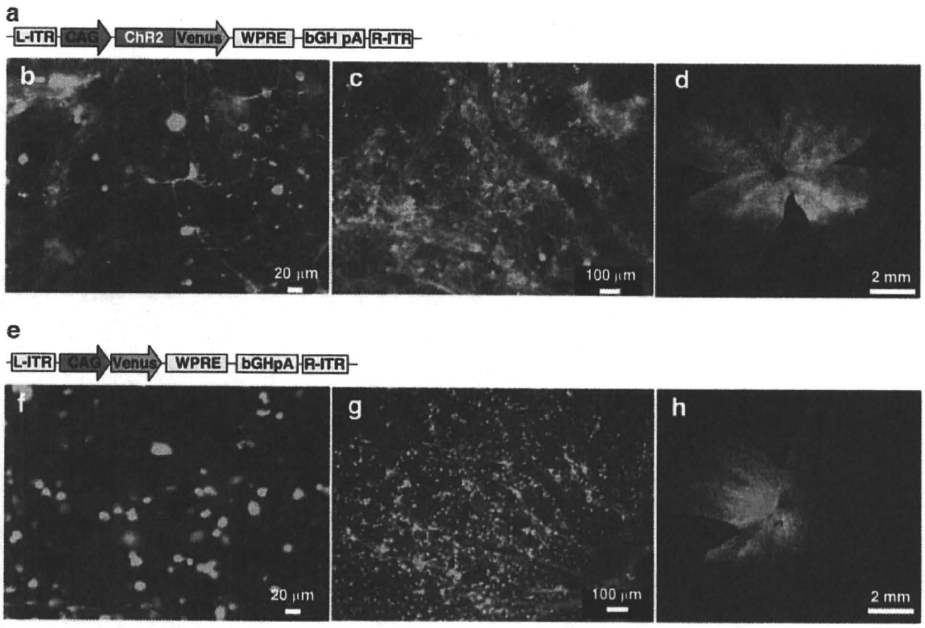

Figure 3 Expression profiles of the rAAV-derived proteins in the retina. Construction of the rAAV vector expressing ChR2V (**a**) and Venus (**e**) is illustrated. After 6 months of intra-vitreous injection, the rAAV-derived protein expression in whole-mounted retinal samples was observed by fluorescence microscopy. ChR2V expression was observed in the membrane (**b–d**) and Venus was expressed in the cytoplasm (**f–h**) of the retinal cells.

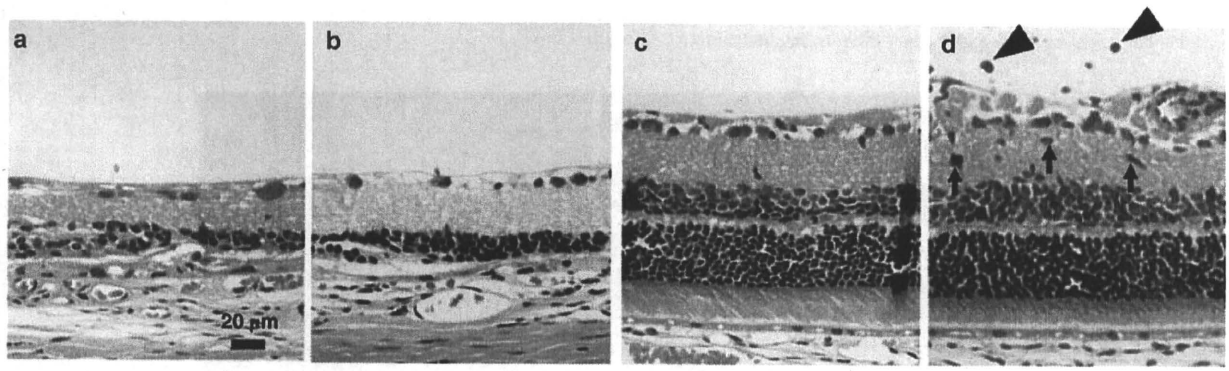

Figure 4 Histological examination of rAAV-ChR2V-treated retina. rAAV-ChR2V was administered by intra-vitreous injection into the left eye of RCS (*rdy/rdy*) rats. After 64 weeks, their right (control) (**a**) and left (**b**) eyeballs were enucleated and stained with hematoxylin and eosin. As a model of inflammation, age-matched RCS (+/+) rats were administered lipopolysaccharide (LPS) by intra-vitreous injection and their eyeballs were enucleated after 48 h. Retinal sections of untreated RCS (+/+) (**c**) and the LPS-treated (**d**) rats were studied. Substantial infiltration of inflammatory cells, which were mainly PMNLs in the neural retina (arrow) and vitreous humour (arrowhead), was observed in the retina of the LPS-treated rats.

after the development of EIU. Our study demonstrated that EIU caused leucocyte adhesion in the retinal venules (Figures 6c and d). However, there was no difference in leucocyte adhesion between the untreated (Figure 6a) and the rAAV-ChR2V-injected (Figure 6b) RCS rats, which had received the rAAV injection 1 year previously.

Humoral immune responses to the viral vector and transgene

To assess the possibility of a systemic humoral immune response to the viral vector or transgene, we determined the antibody levels against the rAAV2 capsid and ChR2 in serum by enzyme-linked immunosorbent assay. In the rAAV-ChR2V-injected rats, rAAV2 capsid-specific antibodies were detected and showed the maximum production at 2 months after injection (0.01–12.21 $\mu g\,ml^{-1}$; Figure 7a). However, the titre was extremely low in this study compared with that in a previous report of intramuscular injection of AAV2 (200–400 $\mu g\,ml^{-1}$).[16] The titre against the ChR2 protein was the maximum at 6 months post-injection. However, this level was also low (0–4.77 ± 2.55 $\mu g\,ml^{-1}$) compared with the antibody level in serum of the immunized rabbit (1442.34 $\mu g\,ml^{-1}$), which received a peptide injection to produce antibody to ChR2 forcibly (Figure 7b).

Analysis of T-lymphocyte subsets

Total T lymphocytes were gated with positive staining of anti-CD3. Then, the population of lymphocytes was confirmed by forward scatter (cell size) versus side scatter (cell granularity). Analysis of T lymphocyte subsets, namely $CD4^+$ (T helper cells), $CD8^+$ (cytotoxic

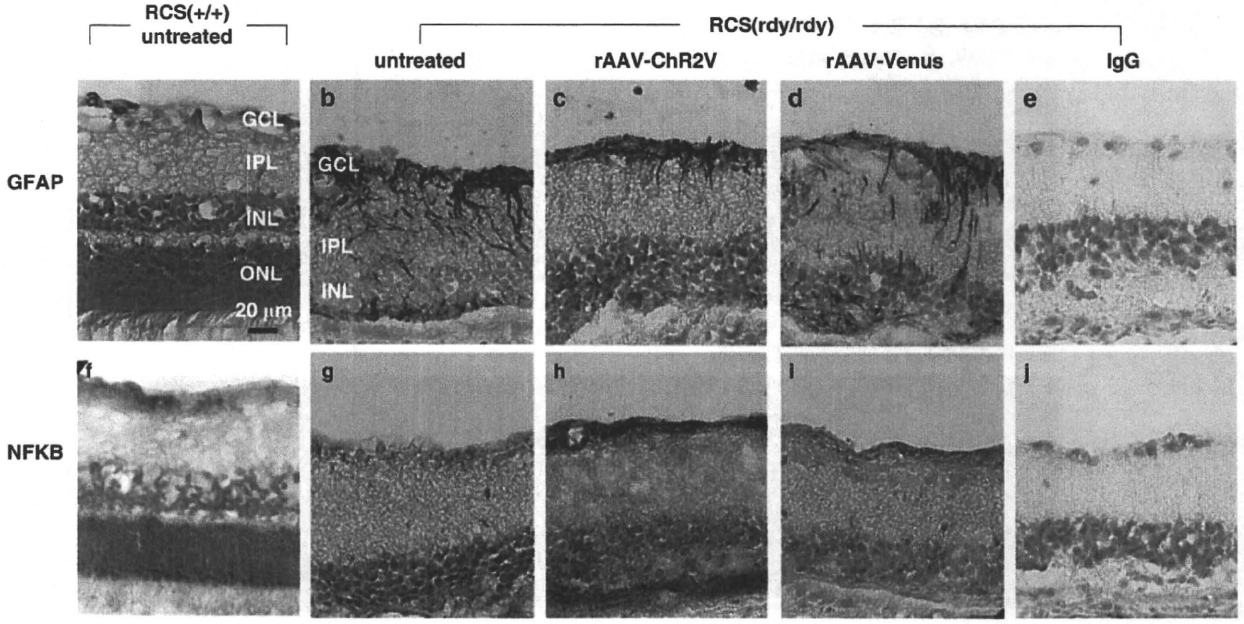

Figure 5 Changes in the protein immunoreactivities in the retina. Untreated RCS (+/+) (**a** and **f**) and RCS (*rdy/rdy*) (**b** and **g**) rats were used as the controls. rAAV-Venus (**d** and **i**) or rAAV-ChR2V (**c** and **h**) was administered by intra-vitreous injection into the left eye of RCS (*rdy/rdy*) rats. After 64 weeks, their eyeballs were enucleated. All the RCS rats were of the same age at the time of enucleation (2.2 years). As the negative control for staining, the first antibodies were replaced with non-immune mouse immunoglobulin G (**e** and **j**). DNA was counterstained with 4', 6-diamidino-2-phenylindole. GFAP expression was restricted to the ganglion cell and nerve fibre layers of the ChR2V-treated retina (**c**); however, it was observed throughout the inner half of the retina in the untreated RCS (**b**) and rAAV-Venus-injected RCS (**d**) rats. Nuclear factor-κB expression was restricted to the ganglion cell layers in all the tested RCS rats, but it was markedly high in the ChR2V-treated retina (**h**).

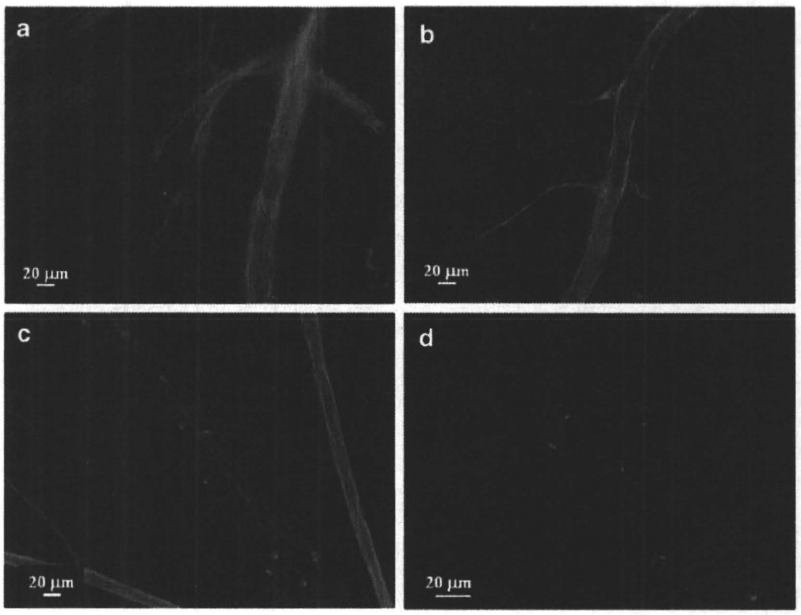

Figure 6 Adverse effect of rAAV-ChR2V treatment on retinal leucocyte adhesion. To study the adverse effect of ChR2 treatment in RCS rats, their retinas were examined after 1 year of rAAV-ChR2V injection. As a model of inflammation, RCS (+/+) rats received an intra-vitreous injection of lipopolysaccharide (LPS) and were examined 48 h after the injection. Flat-mounted retinas labelled with concanavalinA lectin showed increased number of adherent leucocytes in the retinal vessels of the LPS-injected rats (**c**) compared with the untreated (**a**) and rAAV-ChR2V-injected (**b**) rats. High-magnification photography of the LPS-treated retinal vessels showed leucocyte adhesion more clearly (**d**).

cells) and $CD4^+CD25^+$ (T regulatory cells), was performed. The $CD4^+/CD8^+$ ratio is a known indicator of the immunoregulatory status.[17,18] Our results demonstrated that the $CD4^+/CD8^+$ ratio after 1 week of the rAAV injection was higher than the pre-injection ratio (Figure 8a). This increase occurred in the case of both the rAAV-Venus and rAAV-ChR2V injections. In addition, the $CD4^+/CD8^+$ ratio only 1